Available online www.jsaer.com

***Journal of Scientific and Engineering Research*, 2023, 10(7):1-8**

Research Article

ISSN: 2394-2630
CODEN(USA): JSERBR

Analysis and Simulation of Electromechanical Parameters of the Cage Asynchronous Motor of Carrigres during No-load Operation

Kabimba Mupa[1], Lionel Nkouka Moukengue[1], Flory Lidinga Mobonda[1], Narcisse Meni Babakidi[2], André Bandekela Kazadi[2], D. Lilonga-Boyenga[1]

[1]Laboratory of Electrical and Electronic Engineering, ENSP, Marien Ngouabi University, Congo
[2]Laboratory of Electrical and Electronic Engineering, ISTA-Kinshasa, Democratic Republic of Congo

Abstract In this article, we present and address the model of the squirrel cage asynchronous motor during no-load starting. The no-load run is a period that allows us to validate the electromechanical parameters of the asynchronous motor when no mechanical load is applied on its rotor; this allowed us to take measurements of the stator current and the rotor speed to validate them with the model. The purpose of this article is to validate the model of the asynchronous cage machine, and to analyze the behavior when the machine is fed directly from the electrical network.

Keywords Electromechanical parameters, Asynchronous motor with cage, Carrigres, No-load operation.

1. Introduction

In industrialized countries, about 70% of the electrical energy produced is used by electric motors. In addition, more than 60% of all electrical energy converted into mechanical energy is consumed by pumps and fans that are driven by induction motors [1]. However, the realization of accurate drive torque command is the major drawback of these induction machines. From an automation point of view, the asynchronous motor (AMS) is a dynamic system that poses a number of control problems because of its characteristics: a nonlinear, multivariable, and highly coupled system whose resistive and inductive parameters vary as well as the load. Moreover, some variables are not measurable, in particular the fluxes [2]. In industry, more than half of the electrical energy produced is consumed by electric motors. Among several types of electric motors, the three-phase asynchronous machines are the most used.

Predicting the behavior of an electrical machine, and in particular the asynchronous machine with cage, often requires a mathematical modeling of it in dynamic and steady state, then simulation of the operating mode relative to the healthy state and under the constraint of intrinsic or extrinsic defects. At the beginning of the nineties, an appropriate model was published based on a multi-winding structure of the rotor cage and taking into account the discrete character of the winding distribution on the periphery of the stator [3-10].

After the identification of the parameters of the asynchronous machine from the test bench, a simulation phase was necessary in order to verify the validity of the model and possibly adjust its parameters if necessary. For this purpose, we introduced the identified parameters into a Matlab/Simulink simulation model. It is then necessary to compare the results of the simulation with the experimental measurements carried out under the same conditions. The asynchronous machine, whose parameters were identified in the previous section, is supplied directly by the balanced three-phase network at a voltage of 400V with a frequency of 50 Hz for a no-load test. The simulation results give the behavior of the evolution of the fundamental quantities (electromechanical parameters) of the asynchronous machine; in particular phase currents, electromagnetic torque, motor speed and magnetic flux.

2. Theory

2.1 Characteristics of the chosen asynchronous motor

i. Nominal power: 5,5 kW
ii. Nominal voltage: 380V
iii. Nominal current: 10A ;
iv. Speed of rotation: 1450 tr/min
v. Power factor: 0,85

2.2 Autotransformer characteristics

i. DE LORENZO brand, DL 2025
ii. Nominal power: 20Kva
iii. Input voltage: 380V
iv. Output voltage (variable): 0 à 440V +
v. Neutral
vi. Output voltage (fixed) : 380V + neutral
vii. Rated current: 45A

2.3 Model of the equations

Motor parameter equations

The stator losses in a three-phase machine are obtained by the expression:

$$P_{jst} = 3R.I_{ph}^2 \quad (1)$$

$$R_s = \frac{U}{I_{ph}} \quad (2)$$

Variation of the resistance of the stator windings

We have the stator joule losses in a three-phase machine, for an unstable regime, this loss will be obtained by the following expression:

$$R_s = \frac{U}{I_{ph}} \quad (3)$$

Torque versus voltage equations

$$\mathrm{C_m} = \mathrm{k.U^2} \quad (4)$$

Equations of the torque as a function of the absorbed current

The torque versus current is obtained by the following expression

$$\mathrm{C_m} = \mathrm{k}.C_{st} \quad (5)$$

Determination of mechanical parameters: J, f

The identification of the mechanical parameters J and f (respectively moment of inertia and viscous friction coefficient) is based on the measurement of the mechanical losses when the machine rotates at a given speed and is done by measuring the speed as a function of time during deceleration. The moment of inertia J can be calculated by:

$$J = \frac{P_{méc}}{\Omega_n\left(\frac{d\Omega}{dt}\right)_{\Omega=\Omega s}} \quad (6)$$

This relationship shows that the measurement of the moment of inertia J depends on the precision with which the mechanical power is determined. The measurement of the deceleration curve and its approximation by an analytical function allows to calculate the derivative of the velocity:

$$\frac{d\Omega}{dt} = 2\pi \frac{\Delta N}{\Delta t}\frac{1}{60} \quad (7)$$

$$\Omega_n = 2\pi \frac{N_n}{60} \quad (8)$$

3. Analysis of motor no-load tests

3.1 Current measurement

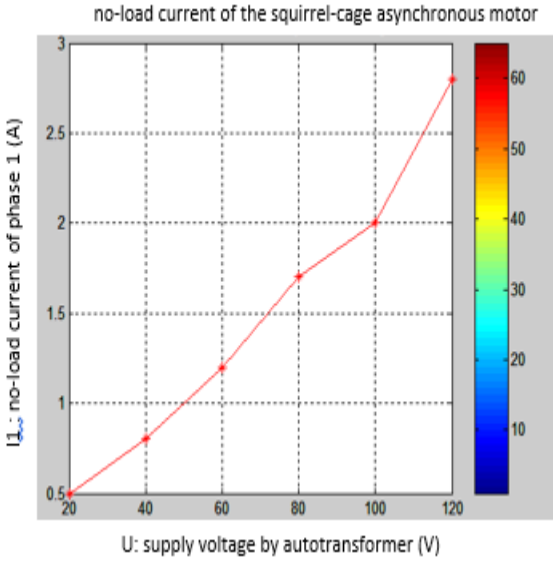

Figure 1: No-load current of phase 1

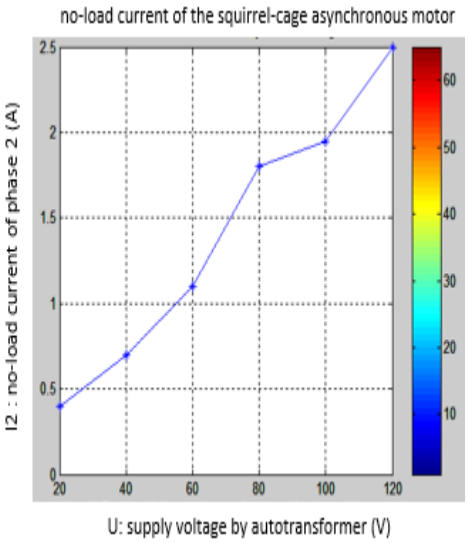

Figure 2: No-load current of phase 2

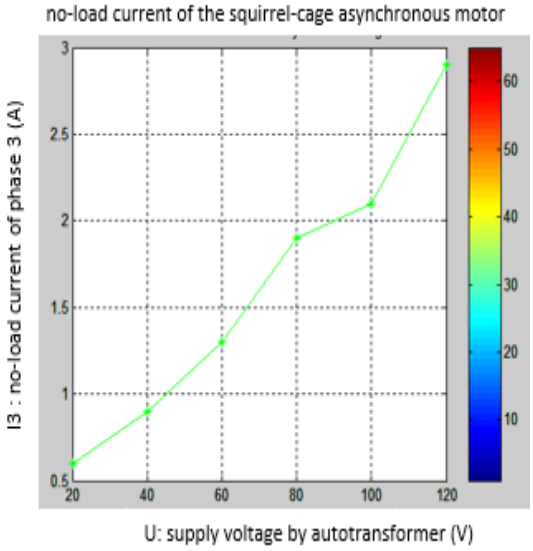

Figure 3: No-load current of phase 3

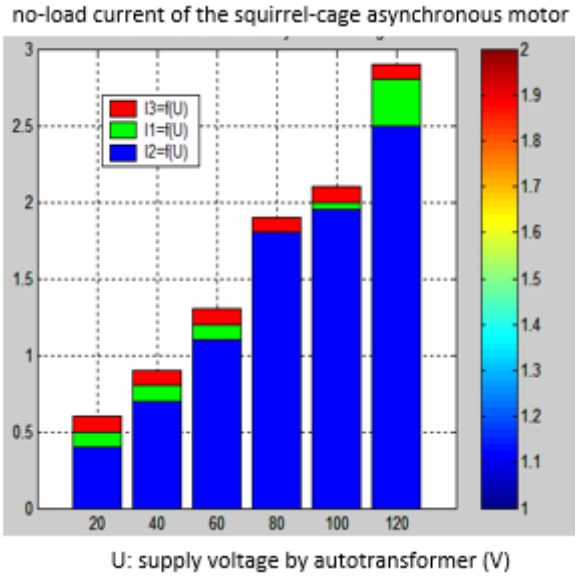

Figure 4: No-load current of phases

The bars of the simulations show the different current points. The red bar describes the behavior of the current of the third phase, which grows under the interval of 0.6 A until 2.9 A (figure1). The blue bar describes the behavior of the current of the second phase, which grows under the interval of 0.4 A until 2.5 A (figure 2 (figure 3). The green bar describes the behavior of the current of the first phase, which increases under the interval of 0.5 A up to 2.8 A. All these currents are function of the variation of the voltage of the autotransformer, within the framework of the test without load as shown in Figure 4.

3.2 Stator losses

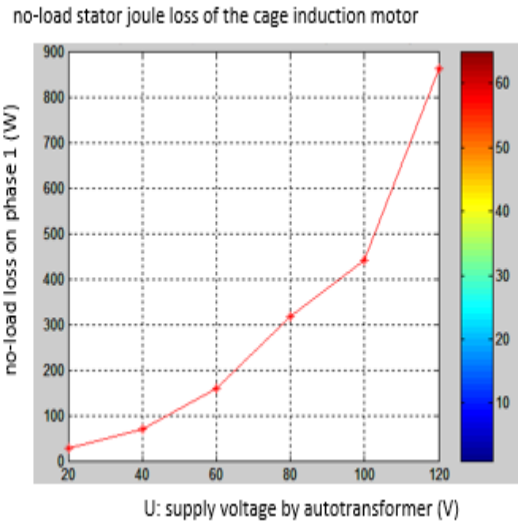

Figure 5: Determination of joule losses of phase 1

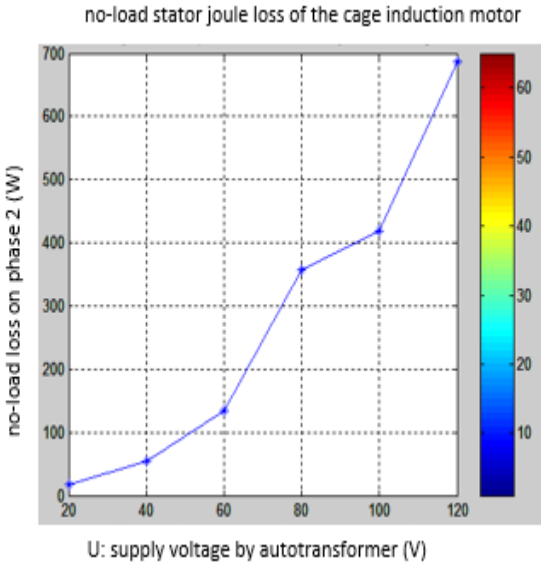

Figure 6: Determination of joule losses of phase 2

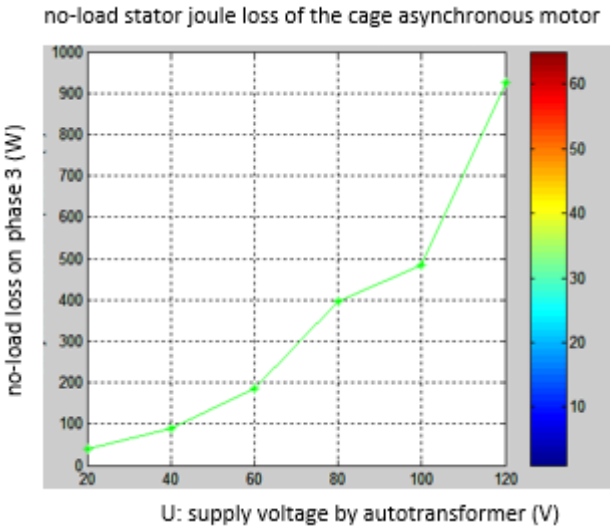

Figure 7: Determination of Joule losses of phase 3

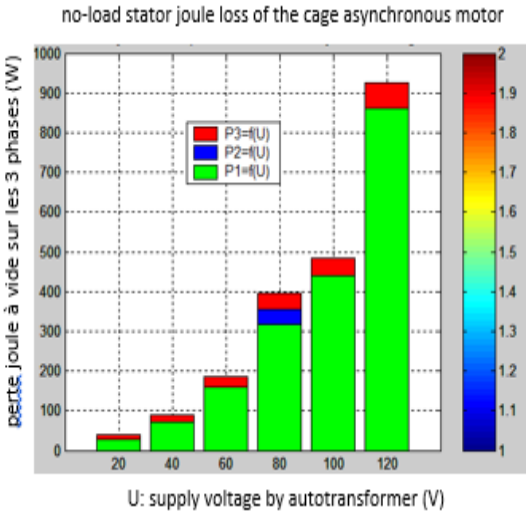

Figure 8: Determination of Joule losses of three phases

The bars of the simulations give the different points of the joule losses. The red bar describes the joule loss behavior of the third phase, which increases under the interval of 39.6W to 925.1W (figure 5). The blue bar describes the Joule loss behavior of the second phase, which increases under the interval of 17.6 W up to 687.5W as illustrated in figure 6. The green bar describes the Joule loss behavior of the first phase, which increases under the interval of 39,6 W up to 925,1 W (figure 7). All these currents are function of the variation of the autotransformer voltage, within the framework of the no load test as illustrated in figure 8.

3.3 Stator resistors

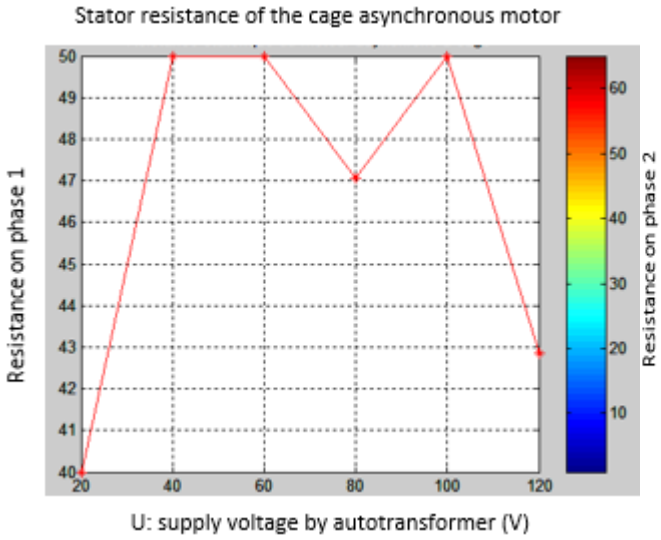

Figure 9: Determination of the resistance on phase 1

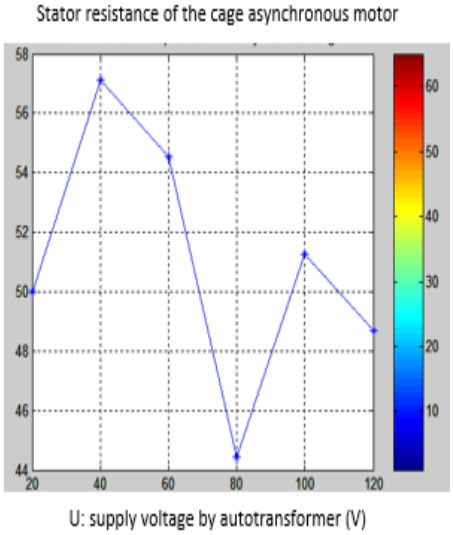

Figure 10: Determination of the resistance on phase 2

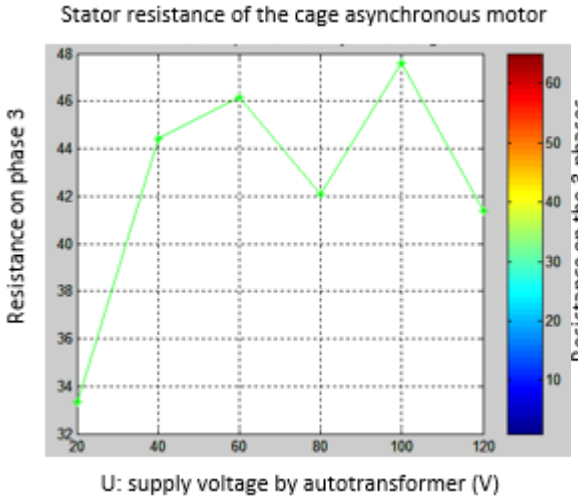

Figure 11: Determination of the resistance on phase 3

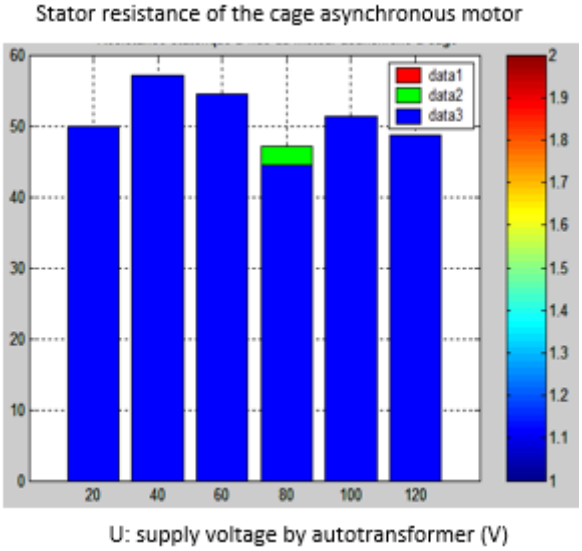

Figure 12: Determination of the resistance on phases

The bars in the simulations give the different points of the stator resistances. The red bar describes the resistance behavior on the third phase, which grows under the interval of 33.33 Ω up to 41.37 Ω as illustrated in figure 9. The blue bar describes the resistance behavior on the second phase, which grows under the interval of 50 Ω up to 48 Ω (figure 10). The green bar describes the resistance behavior on the first phase, which grows under the interval of 40 Ω up to 42.85 Ω as illustrated in figure 11. all these currents are function of the variation of the autotransformer voltage, under the no-load test as illustrated in figure 12.

4. No-load operation

Matlab/Simulink model of the asynchronous cage machine

The purpose of this simulation is to validate the model of the asynchronous machine, and to analyze the behavior when the machine is fed directly from the standard grid. Figure 13 represents the Matlab/Simulink model of the asynchronous motor described by the previous equations. It consists of the three-phase power source block, the abc/dq transformation block and the state model block of the induction machine (IM)

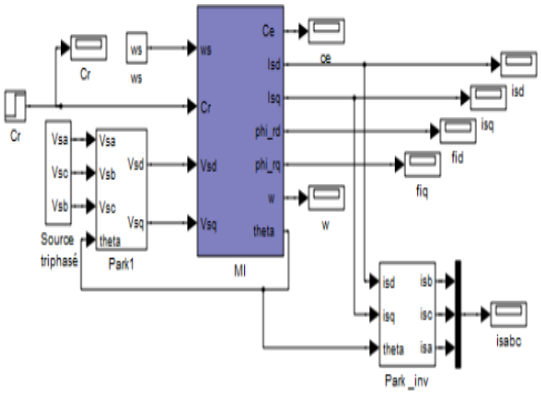

Figure 13: Matlab/Simulink model of the asynchronous motor

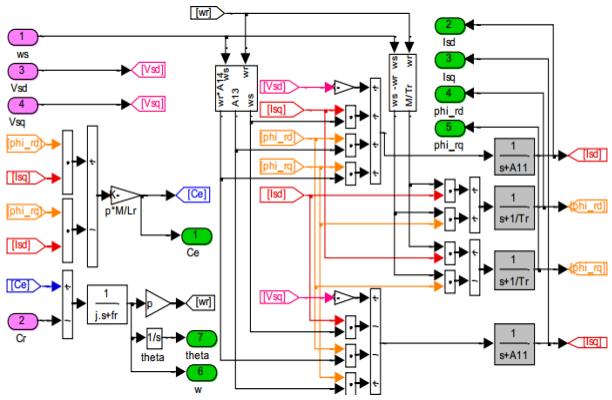

Figure 14: Content of the block (IM)

Simulation of electromechanical parameters

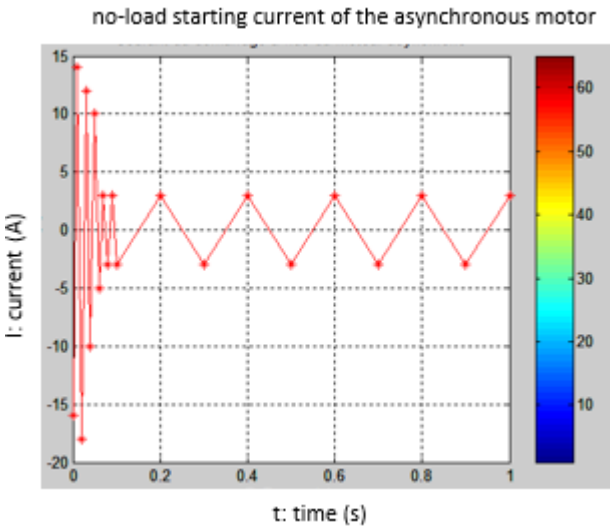

Figure 15: Behavior of the stator current

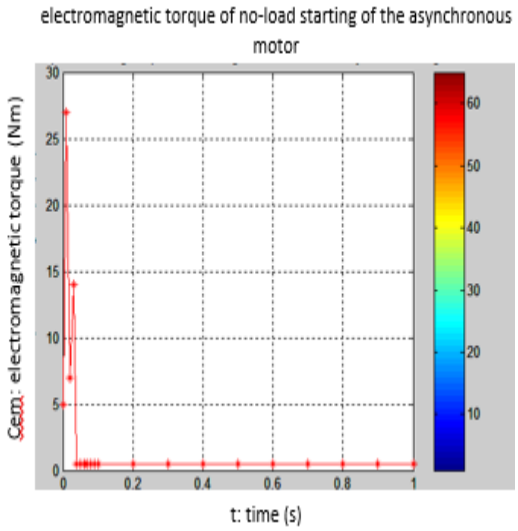

Figure 16: Behavior of the electromagnetic torque

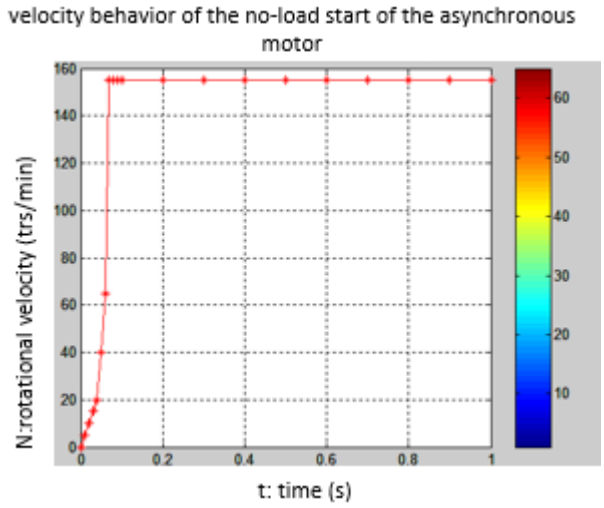

Figure 19: Velocity behavior

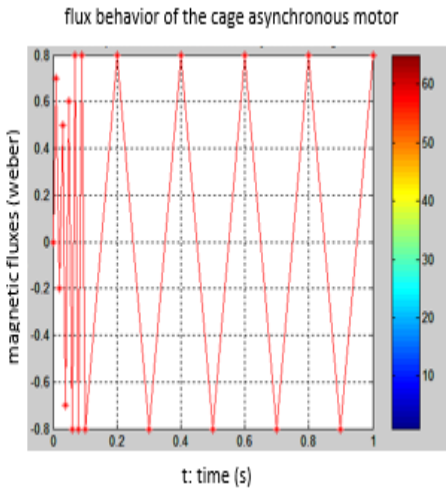

Figure 20: Flux behavior

The results of the nominal values of the simulated machine are equal to the real values of the machine on the test bench and the simulation during the no-load start-up, show that in transient regime (lower than 0.1s), the

quantities of the machine (current, torque,...) present oscillations and overshootings in this interval and after this time, the machine functions in the permanent regime (figure 13 and 16).

Validation of the parameters with a start-up test

By performing a no-load direct start test of the asynchronous machine, the stator phase current response and the mechanical speed were recorded during the transient and steady state regimes in order to make a comparison. The experimental measurements and the curves simulated by the identified parameters were superimposed on the same graph, which validates the identified parameters.

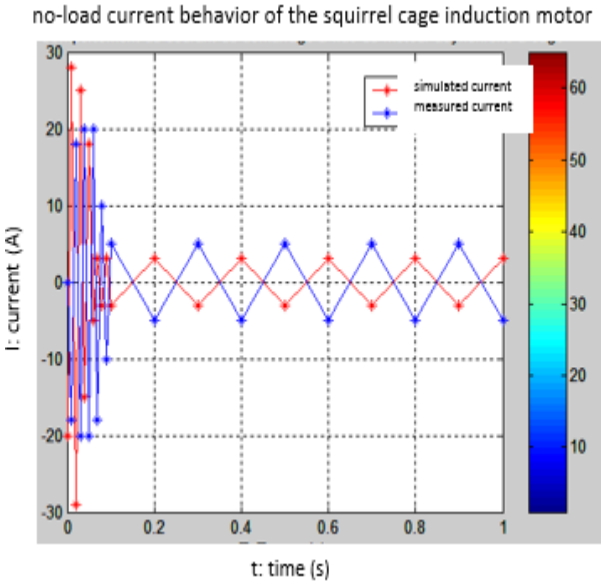

Figure 21: Current "i_{sa}" measured and simulated during a no-load start

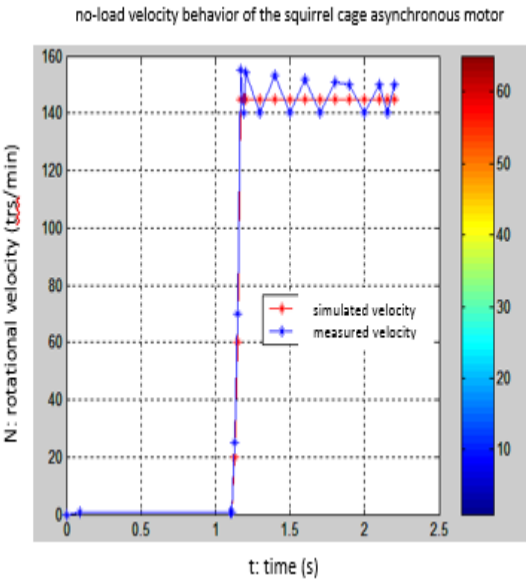

Figure 22 : Rotor speed "N_r" measured and simulated during a no-load start

5. Conclusion

In this article, we have carried out the no-load and cage synchronous motor tests in the ISTA-Kinshasa electrical machines testing laboratory. These tests made it possible to describe the behavior of the values of the various electrical parameters (Rs, Ls, Rf) and mechanical (J, f), of the asynchronous motors which drive the machines of Carrigres, starting from the test benches, based on the one hand on the voltammetric method and that of two wattmeters and on the other hand on the measurement of the mechanical losses when the machine turns at a given speed according to the time at the time of the slowdown. A simulation phase using Matlab-simulink software was necessary in order to verify the validity of the experimental measurements taken on the test bench during the no-load and load operation of the engine and to analyze its behavior when it is fed directly by the network.

References

[1]. Dheeraj Josh1, Meghna Gill « comparison of vector control techniques for induction motor drive », Indian Journal of Electrical and Biomedical Engineering, Volume.1 Number.1, pp.17-27, January-June 2013

[2]. RICARDO Alvarez Salas, « développement de lois de commande avec observateurs pour machine asynchrone », thèse de doctorat, Institut National Polytechnique de Grenoble, 2002

[3]. B. Cart, V. Gosseaume, F. Kogut-Kubiak , M.H. Toutin (Céreq), "La maintenance industrielle; une fonction en évolution, des emplois en mutation," BREF Centre d'études et de recherches sur les qualifications, Céreq Bref, no. 174, Marseille, Avril 2001.

[4]. H. Toliyat, T.A. Lipo, "Transient analyze of induction machines under stator, rotor bar and end ring faults", IEEE Trans. Energy Conv. vol. 10, no. 2 , pp: 241-247 , 1995.

[5]. G. Didier, E. Ternisien, O. Caspary, H. Razik ,¨A new approach to detect broken rotor bars in induction machines by current spectrum analysis¨, Journal of Mechanical Systems and Signal Processing (MSP), vol. 21, n° 2, pp. 1127-1142, Feb.2007.

[6]. R. N. Andriamalala, H.Razik, L. Baghli, F-M. Sargos ,¨Eccentricity Fault Diagnosis of a Dual-Stator Winding Induction Machine Drive Considering the Slotting Effects¨, IEEE Transactions on Industrial Electronics, Volume 55, Issue 12, , pp. 4238 – 4251, Dec. 2008.

[7]. J. S. Thomson, C. S. Kallesoe, ”Stator fault modelling of induction motors”, SPEEDAM Conferance, 2006.

[8]. J. S. Thomson, C. S. Kallesoe,” Stator fault modelling of induction motors”, SPEEDAM Conferance, 2006.

[9]. R.M. Tallam, Sang Bin Lee, G.C. Stone, G.B. Kliman, Jiyoon Yoo, T.G.Habetler, R.G. Harley, "A Survey of Methods for Detection of Stator-Related Faults in Induction Machines", Industry Applications, IEEE Transactions on , vol.43, no.4, pp.920-933, July-Aug. 2007.

[10]. Jean Pierre CARON, Jean-Paul HAUTIER « Modélisation et commande de la machine asynchrone » Editions Technip, 1995, ISBN 2-7108-0683-5 – p.13-28, p.76-82

[11]. G. CLERC, M. BESSAOU, P. SIARRY, P. BASTIANI. Identification des machines synchrones par algorithme génétique. Revue RIGE, Volume 5 - N° 3-4/2002, p. 485-515, 2002

[12]. Luc LORON. Identification paramétrique de la machine asynchrone par filtre de Kalman étendu Revue Internationale de Génie Electrique, AC 3, n°2 – p. 163-205, 2000